Hearing Research 466 (2025) 109382

Contents lists available at ScienceDirect

Hearing Research

journal homepage: www.elsevier.com/locate/heares

Research Paper

Intracochlear electric potential measurements for estimating electrode array position in cochlear implantation: The *in vivo* utility of an *ex vivo* model

Samuel Söderqvist [a,b,*], Ville Sivonen [a], Alexander Huber [c], Saku T. Sinkkonen [a], Leanne Sijgers [c]

[a] Department of Otorhinolaryngology – Head and Neck Surgery and Tauno Palva Laboratory, Head and Neck Center, Helsinki University Hospital and University of Helsinki, Helsinki, Finland
[b] Department of Otorhinolaryngology – Head and Neck Surgery, Turku University Hospital, Turku, Finland
[c] Department of Otorhinolaryngology, Head and Neck Surgery, University Hospital Zurich, University of Zurich, Zurich, Switzerland

ARTICLE INFO

Keywords:
Cochlear implants
Intracochlear electric potentials
Transimpedance matrix
Electrode-to-medial-wall distance
Cochlear dimensions

ABSTRACT

Introduction: Stimulation of cochlear implant electrodes generates intracochlear electric potentials. The local electric potentials can be assessed using *e.g.* transimpedance matrix (TIM) and four-point impedance (Z_{fp}). Both of these measurements are dependent on the cochlear dimensions and the distance between the electrode and the medial wall of the scala tympani (d_{EM}). In a recent temporal bone study, a model based on electric potential measurements gave good predictions of scalar cross-sectional area (A_{scala}) and d_{EM}. The purpose of this study was to further improve this model and evaluate its clinical usefulness. To this end, the intraoperative TIM and Z_{fp} measurements from cochlear implant patients were used as independent variables in the model to predict their A_{scala} and d_{EM} at each electrode contact, which were then compared to those measured from postoperative cone-beam computed tomography (CBCT) images.

Methods: In an earlier study, six cadaveric temporal bones were sequentially implanted with three different electrode arrays: a lateral-wall electrode array, Slim Straight, and two precurved perimodiolar electrode arrays, Contour Advance and Slim Modiolar (Cochlear Ltd, Sydney, Australia). The TIM and Z_{fp} measurements were performed alongside CBCT imaging, from which the A_{scala} and d_{EM} at each electrode contact were measured. From the TIM measurements, the peak amplitudes and decay rate of the electric potentials (EP_{slope}) were computed. In this follow-up study, the statistical modeling of the *ex vivo* measurements was refined to better account for individual characteristics by employing mixed-effect models to predict the A_{scala}s and d_{EM}s. Then, *in vivo* recordings from thirteen patients, of which six were implanted with the Slim Straight and seven with the Contour Advance electrode arrays, were retrospectively analyzed. The A_{scala}s and d_{EM}s were measured from their postoperative CBCT images in a similar manner to the temporal bones. To validate the mixed-effects models developed with the temporal bone data, the patients' intraoperative TIM and Z_{fp} measurements were used as independent parameters in the models to predict their A_{scala}s and d_{EM}s. Finally, the TIM and Z_{fp} parameters measured *in vivo* and *ex vivo* and the measured and predicted A_{scala}s and d_{EM}s were compared using *t*-tests. Also, Pearson's correlation coefficients were computed between the measured and predicted *in vivo* A_{scala}s and d_{EM}s.

Results: Both the amplitudes, indicating electric potential peaks, and Z_{fp}s, reflecting local potential differences, were lower *in vivo* than *ex vivo* (790 vs. 1090 Ω and 253 vs. 270 Ω, respectively, $p < 0.001$ for both), but no differences were detected in the decay of the electric potentials. In addition, the *in vivo* Z_{fp}s were lower, and the electric potential decay was slower with the lateral wall (Slim Straight) compared to perimodiolar (Contour Advance) array (234 vs. 284 Ω and −94 vs. −160 Ω/mm, $p < 0.001$ for both). The mixed effects models with and without random effects explained 73 % and 51 % of the variance, respectively, for A_{scala}. The mean absolute error between measured and predicted A_{scala}s was 12 %. For d_{EM}s, the corresponding percentages were 65 %, 50 %, and 51 %. The correlations between the patients' measured and predicted A_{scala}s and d_{EM}s were $r = 0.60$ and $r = 0.48$ ($p < 0.001$, for both). When compared in the basal, middle, and apical sections, the predicted A_{scala}s differed

* Corresponding author at: Department of Otorhinolaryngology – Head and Neck Surgery and Tauno Palva Laboratory, Helsinki University Hospital, Kasarmikatu 11-13, 00130 Helsinki, Finland.
E-mail address: samuel.c.soderqvist@utu.fi (S. Söderqvist).

https://doi.org/10.1016/j.heares.2025.109382
Received 11 May 2025; Received in revised form 30 July 2025; Accepted 30 July 2025
Available online 4 August 2025

significantly from the measured values only in the middle section of the array (4.0 ± 0.48 mm *vs* 3.50 ± 0.36 mm, $p < 0.001$). For d_{EM}s, the model gave too large estimates in the apical section of the array (1.04 ± 0.49 mm *vs.* 1.52 ± 0.48, $p < 0.001$).

Conclusion: The A_{scala} at each electrode contact can be estimated using the TIM and Z_{fp} measurements, which may help verify the correct alignment of the electrode array during the surgery. While the measured and predicted d_{EM}s correlated with each other, there were significant differences between their absolute values. Given the large variation in d_{EM}s for different array types, electrode-specific d_{EM}s models could improve the accuracy of the predictions.

1. Introduction

Cochlear implants (CIs) enable hearing with electrical stimulation of the spiral ganglion neurons (SGNs) in the inner ear. For the stimulation to be meaningful, first, the sound waves are gathered by the external microphones and processed into a digital signal. The signal is then transmitted to the internal receiver-stimulator and ultimately conveyed to the electrode array in the cochlear duct, usually laying within the scala tympani. One of the key anatomical and physiological factors enabling the function of a CI is the tonotopic organization of the cochlea; sensations of high and low frequencies are generated by stimulating the electrode contacts in the basal and apical sections of the electrode array. When the electrodes are stimulated in a monopolar fashion, as they are in most clinical settings, the current is applied between an intracochlear electrode and an extracochlear reference electrode. Due to broad monopolar stimulation and the poor conductivity of the structures surrounding the scala tympani, only a fraction of the stimulation current reaches the SGNs, which are separated from the scala tympani with a thin bony wall (Briaire and Frijns, 2000; Tran et al., 2015). The rest of the current mainly flows out of the cochlea through its walls or via the scala tympani towards its base (Vanpoucke et al., 2004a; Tran et al., 2015; Aebischer et al., 2021). Thus, the neural populations targeted by stimulation at each electrode partially overlap with those of their neighboring contacts, limiting the number of independent channels. This remains one of the major limitations of CI technology today (Friesen et al., 2001; Bingabr et al., 2008; Landsberger et al., 2012; Joly et al., 2021).

As a higher number of independent channels is associated with better hearing outcomes, especially in background noise (Friesen et al., 2001), several methods have been investigated to reduce channel interaction. One of the proposed methods is to deactivate electrode contacts based on their intracochlear location in CI programming. The deactivation of electrode contacts, which are farther away from the modiolus (as measured by the electrode-to-medial wall distance, d_{EM}), evaluated from computed tomography (CT) images, than their neighboring contacts, improved pitch perception in a study by Labadie et al. (2016).

Channel interaction can be influenced by both pre- and intra-operative factors. When the electrode array is positioned closer to the medial wall of the scala tympani, electrode discrimination and speech recognition may be better (Ramos de Miguel et al., 2018; Peters et al., 2019; Heutink et al., 2021; Ding et al., 2023; Collins et al., 2024). However, not all studies have found these relationships (*e.g.* Fitzgerald et al., 2007). Thus, channel interaction may be reduced by choosing a perimodiolar array that brings the stimulating contacts closer to the SGNs than for lateral wall arrays. In two experiments, the extent of neural activation was more focused after stylet removal (*i.e.*, the array was shifted to a more modiolar position) of perimodiolar electrode arrays (Cohen et al., 2003; Van Weert et al., 2005). The surgical technique may also play a role in channel interaction. When the round window approach is chosen over insertion via a cochleostomy, the electrode array may lie closer to the modiolus and is more likely to remain in the scala tympani during the insertion (Wanna et al., 2014; Jiam et al., 2016; Avasarala et al., 2021). These factors are either irreversible or their alterations require reimplantation, emphasizing the pre-operative planning and decision-making during surgery.

In addition to their primary function, modern CIs are equipped with versatile back-telemetry tests that can be used to verify device integrity, such as monopolar contact impedance measurements. They also allow measurement of the stimulation-induced intracochlear electric potentials along the electrode array by measuring the potential difference between the non-stimulating intracochlear electrodes and an extracochlear reference electrode. Depending on the CI manufacturer, these current-induced electric potentials on non-stimulating contacts are referred to as “transimpedances”, which we will use throughout this manuscript, or as electric field imaging or impedance field telemetry. Since their introduction, the applications of the monopolar impedance measurements have expanded. For example, they can be used to evaluate the physical surroundings of the electrode array, such as the development of fibrous tissue or ossification and insertion depth, scalar translocation from the scala tympani to scala vestibuli, or electrode migration out of the cochlea (Dietz et al., 2016; Wilk et al., 2016; Helmstaedter et al., 2018; Giardina et al., 2018; Aebischer et al., 2021; Dong et al., 2021; Schraivogel et al., 2023; Zhang et al., 2024; Kopsch et al., 2024). Transimpedances have been used to investigate intracochlear current pathways that have, for example, helped to identify and deactivate channels causing facial nerve stimulation (Vanpoucke et al., 2004a; Vanpoucke et al., 2004b; Saoji et al., 2024). These measurements are also utilized to detect electrode array insertion problems, such as electrode tip fold-overs and incomplete array insertions, more specifically than what can be inferred from monopolar contact impedances (Vanpoucke et al., 2012; Zuniga et al., 2017; de Rijk et al., 2020). Many CI manufacturers visualize transimpedance measurements as two-dimensional heatmaps or voltage matrices, such as the transimpedance matrix (TIM), across all possible combinations of the intracochlear electrodes, allowing a visual inspection to detect open or short circuits or typical patterns related to extracochlear electrodes, tip fold-overs, or even anatomical variations (Cottrell et al., 2024). The transimpedances are quick to record during the surgery and post-operative follow-up appointments, and unlike CT scans, they do not expose the patient to radiation.

The transimpedances are also affected by the cochlear geometry and its dimensions, as well as the location of the electrode array (Malherbe et al., 2016; Bai et al., 2019; Lei et al., 2021a; Söderqvist et al., 2022, 2023). Different configurations to measure local electric potentials along the electrode array have become available. These include four-point impedance (Z_{fp}) measurement, in which a configuration of four adjacent electrodes is used with current flowing between the two outermost electrodes, and electric potential is measured between the contacts in the middle. Depending on the CI manufacturer, Z_{fp} measurement may be available in the experimental protocols using either their clinical or custom-made software. In Cochlear Nucleus (Cochlear Ltd, Sydney, Australia) devices, the Z_{fp} is termed as bipolar transimpedance and it is available as a research option in the clinical software.

In cadaveric human temporal bones (HTBs), the Z_{fp}s are higher when the d_{EM}s are smaller (Tan et al., 2014; Pile et al., 2017; Söderqvist et al., 2023). Sijgers et al. (2022) demonstrated that over 60 % of the variance in d_{EM} can be accounted for using a combination of insertion depth, monopolar impedance, three-point impedance (in which the stimulation is monopolar, but the resulting potential is measured between two

electrodes adjacent to the stimulating electrode), and Z_{fp} measurements. This suggests that these electric potential measurements can serve as effective predictors of d_{EM} when used intraoperatively, before being affected by potential fibrotic tissue formation or ossification (Leblans et al., 2022; Razmovski et al., 2022; Sijgers et al., 2024). In an earlier HTB study, the cross-sectional area of the bony cochlear duct, including the scala tympani, vestibuli, and media (A_{scala}), at the location of each electrode contact and d_{EM} could be estimated with fair accuracy using information only from the electric potential measurements and insertion depth (Söderqvist et al., 2023). The linear models for these estimations included only fixed effects, assuming that the relationships between electric potential parameters, anatomical dimensions, and d_{EM} are the same for each specimen. However, as individual characteristics, for example, bone density and cochlear dimensions, may affect the intracochlear electric potential measurements, these factors should be considered in the models (Malherbe et al., 2015; Bai et al., 2019; Lei et al., 2021).

The purpose of the current study was to (1) refine the linear regression models developed in Söderqvist et al. (2023) to predict A_{scala}s and d_{EM}s from the electric potential measurements by incorporating individual factors for improved applicability, and (2) verify the model's performance using clinical data. As A_{scala} generally decreases monotonically from the basal to apical direction (Biedron et al., 2010), the developed model may be useful for confirming the correct alignment when a similar pattern in the modeled A_{scala} is observed. In addition, by estimating the d_{EM}, the model may help optimize electrode array placement during the surgery and later assist in CI programming to reduce channel interaction. Further validation is required before these models can be considered for clinical practice.

2. Materials and methods

2.1. Study design and ethics

This study consisted of a retrospective analysis of clinical data from twenty-nine adult patients (age 55.4 ± 16.5 years; mean ± SD), implanted with either a Cochlear Nucleus CI622 Slim Straight or CI612 Contour Advance electrode array (Cochlear Ltd) between October 2023 and June 2024 at the CI center of the University Hospital of Zurich. Thirteen patients were implanted with Slim Straight and sixteen with Contour Advance electrode arrays, each implanted unilaterally. The Slim Straight electrodes were implanted using the round window approach. Five of the Contour Advances were implanted using the extended round window approach and two through a cochleostomy. The study was performed with the approval of the Ethical Committee of Zurich (KEK-ZH 2024–00,881). The utility of the *ex vivo* model (Söderqvist et al., 2023) to predict A_{scala}s and d_{EM}s from the electric potential measurements was assessed for these patients.

2.2. Clinical electric potential measurements

The electric potential recordings were performed with the Custom Sound EP software (version 6.0, Cochlear Ltd.), at the end of the surgery, while the patient was still under general anesthesia and the extracochlear reference electrode was positioned under the temporal muscle (recording mode MP1) for clinical purposes. The measurements were conducted after sealing the inner ear before the skin wound closure. Intraoperative TIM measurements were performed with a maximum current level (CL) that did not exceed 230 CL and did not result in out-of-compliance or saturation. In our subjects, this varied between 172 and 206 CL and was 196 CL on average. The intracochlear electrode array was conditioned by sweeping the contacts with 25 μs wide pulses at 230 CL before the TIM recordings to decrease contact impedances with electrical stimulation. Transimpedance was measured at the end of the first phase of the biphasic stimulation 25 μs wide pulse, marked as "T6" in the Custom Sound EP software.

The Z_{fp}s were measured immediately after the TIM recordings using Custom Sound EP software. At first, electrode 1 was stimulated while electrode 4 was used as a reference, and the potential difference was measured across the electrodes in between them. The configuration of these four electrodes was sequentially moved along the electrode array until electrode 19 was the stimulating electrode and electrode 22 the reference, and measurement was performed between electrodes 21 and 20. The stimulating current was automatically selected by the software and was constant for each patient. The stimulating current varied between 137 and 181 CL, being 156 CL on average. These electric potential measurements were retrospectively collected for further analyses.

2.3. Imaging of the patients

Postoperative CBCT imaging of the cochlea was conducted as part of the clinical routine using the NewTom VGi Evo system (NewTom, Bologna, Italy) in a sitting position with standard clinical parameters, allowing a slice thickness of 0.15 mm. The imaging served to verify correct electrode placement. These CBCT images were reviewed retrospectively, and the width and height of the scalae as well as the d_{EM}s were measured at each electrode contact as described in Söderqvist et al. (2023) using NNT viewer (NewTom, Bologna, Italy). The imaging orientation was set to ensure that the entire cross-sectional area of the scalae and the center of each electrode were visible. The correct view was determined with help of two additional views oriented tangentially to the outer walls of the scalae. All three views were perpendicular to each other. Due to the spiral shape of the cochlea, the orientation was established individually for each electrode contact. The scala width and height were used to calculate the A_{scala}, as the cross-section of the three scalae is approximately an oval.

2.4. Parametrization of the intracochlear electric potentials

In TIM, the transimpedances measured from the non-stimulated electrode contacts represent stimulating-electrode-generated electric potential distributions along the electrode array. However, at the location of the stimulating electrode, the transimpedance includes a reactive component (Vanpoucke et al., 2004a), making it incomparable to the measurements from the non-stimulating contacts. To estimate the electrode-tissue interface without this reactive component, TIM recordings were parametrized based on the measurements from the non-stimulating contacts. Within approximately 0.2–0.4 mm from the stimulating electrode, electric potentials are inversely proportional to the square of the distance, and when the recording contact is located farther away than this, as in both the Slim Straight and Contour Advance electrode arrays, the decay of intracochlear potentials becomes more gradual and follows an exponential pattern (Briaire and Frijns, 2000; Berenstein et al., 2010). Thus, the far-field transimpedance (Z_{far}) can be expressed using Eq. (1), described in Berenstein et al. (2010):

$$Z_{far} = A\, e^{-x/\lambda} + dc \quad (1)$$

where A is amplitude (in Ω), x is the distance (in mm) between the recording electrode contact and the stimulating contact, λ is a length constant, and dc (in Ω) is the direct current offset. As the decrease in electric potentials is asymmetrical, the λs were computed separately for the basal and apical directions. Each profile exhibited a single peak and the dc was assumed to be the similar on the basal and apical sides of the stimulating electrode, resulting in single values for both A and dc. These parameters were optimized to minimize the sum of squares of the error between the measured electric potentials and the modeled, exponentially decaying electric potentials on non-stimulating contacts using the function *fminsearch* in MATLAB (MathWorks, Natick, MA, USA). Further, to emphasize the prominence of each TIM profile and to minimize the effect of extracochlear electrode's location on the transimpedances, the dc component was subtracted from the parametrized

transimpedance values. At the stimulating contact, this was calculated as $Z_{far} - dc$, since $x = 0$, resulting in the amplitude A.

Inspired by Lei et al. (2021), the decay rate of the intracochlear electric potentials (EP_{slope}) at 1 mm from the stimulating electrode in both the apical and basal direction was also estimated. The EP_{slope} was calculated as a derivative of Eq. (1):

$$\frac{d}{dx} A\, e^{-x/\lambda} + dc = -\frac{A}{\lambda} e^{-x/\lambda} \quad (2)$$

When $x = 1$ mm, Eq. (2) becomes:

$$EP_{slope} = -\frac{A}{\lambda} e^{-1/\lambda} \quad (3)$$

where the unit of EP_{slope} is Ω/mm. These analyses were identical to the corresponding analyses for HTBs in Söderqvist et al. (2023). As each profile has a unique EP_{slope} in both the apical and basal direction, the mean of the two was used for the subsequent analyses.

2.5. Statistics

To evaluate the quality of the fit of Eq. (1), the root mean percentage error between the measured and parametrized TIMs was calculated for each patient and stimulating contact. The reference value used to calculate the percentage error and was the mean of the measured transimpedances from the non-stimulating contacts from the corresponding measurement. The electric potential measurements acquired in patients were compared to those from HTBs reported by Söderqvist et al. (2023), as well as across different electrode array types within both groups. As the patients were implanted either with the Slim Straight or Contour Advance electrode array, the HTB measurements with the Slim Modiolar array were excluded from these comparisons. The amplitudes, EP_{slope}, and Z_{fp} were used as dependent variables and patients, HTBs, and electrode array types as independent variables in two-way analysis of variance (ANOVA) in SPSS 29 (IBM, Armonk, NY, USA).

Further, linear mixed regression models were constructed in MATLAB to evaluate electric potential parameters as predictors of A_{scala} and d_{EM}s. In the first part of this analysis, the measurements from the HTBs were used to compute the parameters of the mixed-effects model. In the second part, the clinical electric potential parameters were used as input variables to the model to predict estimates of A_{scala} and d_{EM}s. Finally, the clinically measured A_{scala}s and d_{EM}s were compared to the predicted values to assess the reliability of the model in clinical settings.

In the analysis, a calculated linear insertion depth (d_{ins}) was used to estimate the location of each electrode contact in the cochlea. The distance between the center of each electrode contact and the round window was computed based on electrode array specifications (distance between adjacent electrodes is 0.85–0.95 mm for Slim Straight and 0.81–0.39 mm in the basal to apical direction for Contour Advance). When using d_{ins}, it was assumed that each electrode array was inserted into the cochlea with the insertion mark positioned exactly at the round window or at the cochleostomy. As Z_{fp} is recorded between two adjacent electrodes, for example, electrodes 10 and 11, the corresponding A_{scala}, d_{EM}, amplitude, EP_{slope}, and d_{ins} were defined as the mean of each variable at those electrodes. This approach assigns each set of parameters to the interval between electrode pairs, so the model estimates A_{scala} and d_{EM} between electrodes rather than at individual contacts. For Z_{fp}, the most basal and apical recording electrode pairs were 2–3 and 20–21, respectively, leaving the most basal and apical electrodes out of analyses involving Z_{fp}.

The linear mixed regression analyses were conducted in MATLAB using the function *fitlme* to assess the relationship between the electric potential measurements, A_{scala} and d_{EM}. Further, these models were used to estimate A_{scala}s and d_{EM}s from the clinical electric potential measurements. At first, only the d_{ins} was included in the model to assess its independent contribution. Electric potential measurements were then added to evaluate the extent to which they improve the explained variance of the model. The final regression parameters were obtained using the maximum likelihood estimator. Initially, all fixed effects were considered as potential random effects, grouped by HTB specimen, to discern the most suitable model based on Akaike Information Criterion (AIC) values. Random effects were excluded if either their removal yielded a model with a lower AIC value or the exclusion improved model convergence. For A_{scala}, the resulting linear mixed regression model fulfilling these criteria was outlined in Eq. (4) below:

$$A_{scala} \sim 1 + Z_{fp} + d_{ins} + (1 + Z_{fp} + d_{ins} \mid \mathrm{HTB}) \quad (4)$$

These criteria for the d_{EM} model were met by Eq. (5):

$$d_{EM} \sim 1 \pm Amplitude + EP_{slope} + Z_{fp} + d_{ins} + (1 + Z_{eff} + EP_{slope} + Z_{fp} + d_{ins} \mid \mathrm{HTB}) \quad (5)$$

Finally, marginal and conditional R^2s for both models were computed using the function *r.squaredGLMM* from the *MuMIn* package in R version 4.4.2.

In the second part of the analysis, the linear mixed regression models computed with the HTB measurements were used to estimate the A_{scala}s and d_{EM} based on clinical impedance and insertion depth data using the function *predict* in MATLAB. In addition, correlation coefficients (Pearson's *r*) were computed between the clinically measured and estimated A_{scala}s and d_{EM}s.

Further, the A_{scala}s and d_{EM}s were divided into basal (electrode pairs 2–3 to 7–8), middle (8–9 to 14–15), and apical (14–15 to 20–21) sections. Finally, the absolute value means between measured and predicted values were compared using *t*-tests.

3. Results

This study aimed to evaluate the usefulness of electric potential measurements for assessing the CI electrode array location in clinical settings, using a linear mixed regression model based on HTB measurements.

Each patient was imaged within 1–38 days after the surgery, the mean being 18 days. As each patient was imaged in a sitting position, some scans included both movement and metal artefacts, hindering precise measurements of electrode placement and scalar dimensions. Thus, the A_{scala} and d_{EM} could not be reliably measured for sixteen patients. For thirteen patients (seven implanted with the Contour Advance and six with the Slim Straight electrode arrays), the image quality was considered to be sufficient for reliable measurements. The further analyses were conducted only for these patients. Across all patients and electrode contacts, the average root mean percentage error between the measured and parametrized transimpedances was 2.2 %, with a range from 0.29 % to 6.7 %, indicating good agreement between the measured and computed transimpedances.

3.1. Comparison of electric potential parameters between in vivo and ex vivo

The mean transimpedances over non-stimulating contacts measured for living subjects with the Slim Straight and Contour Advance electrode arrays were 1160 Ω and 1040 Ω, respectively. For the HTBs, the corresponding transimpedances were 1300 Ω and 1210 Ω. When analyzing the computed electric potential parameters with ANOVA, amplitude was lower in living subjects than in HTBs (790 vs. 1090 Ω; $F(1453) = 71.1$, $p < 0.001$). No significant main effects of electrode type or interaction between specimen and electrode type were observed ($F(1453) = 0.11$, $p = 0.74$ and $F(1453) = 0.03$, $p = 0.87$, respectively). In a similar analysis for *in vivo* EP_{slope}, the decay rate was found to be slower in Slim Straight than in Contour Advance (−94 vs. −160 Ω/mm; $F(1416) = 288.7$, $p < 0.001$). Finally, Z_{fp} was lower in living subjects than in HTBs (253 vs.

270 Ω, F(1436) = 5.6, p = 0.018) and when measured using Slim Straight instead of Contour Advance (234 vs. 284 Ω, F(1436) = 5.6, p < 0.001). A statistically significant interaction between the specimen and array type (F(1436) = 4.6, p = 0.033) was found. These results indicate that lower intracochlear electric potentials are generated in living subjects than in HTBs, while the decay rate of the electric potentials is dependent only on the array type (lateral wall or perimodiolar). The local potentials estimated using Z_{fp} are generally lower when measured using a lateral wall electrode array and *in vivo* compared to the perimodiolar electrode arrays and *ex vivo*.

3.2. Prediction of A_{scala} and d_{EM} using linear mixed regression

To predict A_{scala} at the location of the stimulated electrode using only information from the electric potential measurements and d_{ins}, linear mixed regression was conducted. At first, when the d_{ins} was the only independent variable, the conditional and marginal R^2s were 0.67 and 0.27, respectively. When the model was augmented with the electric potential variables, as shown in Eq. (4), the corresponding R^2s were 0.73 and 0.51. For d_{EM}, when the model included only d_{ins}, the conditional and marginal R^2s were 0.142 and 0.138, respectively. When electric potential parameters were included in the model (Eq. (5)), the corresponding R^2s increased to 0.65 and 0.50. The models' parameter estimates, corresponding standard errors, as well as t- and p-values, are found in Table 1.

The linear mixed regression models without the random effects were used to predict A_{scala} and d_{EM} from the clinical electric potential measurements. As seen in Fig. 1A, the predicted and measured A_{scala}s have a strong positive correlation with each other, r = 0.60 (p < 0.001), and Fig. 1B shows that their means increase from apical to basal direction, except for a slight decrease in the measured A_{scala}s between electrode pairs 6–7 and 10–11. Fig. 1C and 1D illustrate the mean and SD of A_{scala} separately for Slim Straight and Contour Advance electrode arrays, respectively. When the measured and predicted A_{scala}s were compared over both array types in the basal, middle, and apical sections of the electrode array (averaged across electrodes 2–7, 8–14 and 15–21, respectively), they were different only in the middle section (4.0 ± 0.48 mm^2 vs 3.50 ± 0.36 mm^2, mean ± SD, p < 0.001). In the basal and apical sections, the corresponding values were 4.16 ± 0.53 mm^2 vs. 4.08 ± 0.32 mm^2 (p = 0.23) and 3.14 ± 0.49 mm^2 vs. 3.08 ± 0.50 mm^2 (p = 0.14). The mean absolute percentage error between measured and predicted A_{scala}s was 12.4 %. The results indicate that predicted A_{scala}s align well with measured values at least in the electrode array's basal and apical regions.

Fig. 2 depicts the comparison of measured and predicted d_{EM}s. When both electrode array types are analyzed together (Fig. 2A), the measured and predicted d_{EM}s show a moderate correlation (Pearson's r = 0.48, p < 0.001). However, when computed separately for each electrode array type, the correlations turn out to be negative for Slim Straight (Fig. 2B, r = –0.13, p = 0.19) and weak for Contour Advance (Fig. 2C, r = 0.26, p = 0.004). The mean absolute percentage error between the measured and predicted d_{EM} was 51.2 %. Figs. 2D–F show the mean d_{EM}s with SDs at separate electrode contacts. In the most apical part of the arrays, the predicted values are larger than the measured ones, and in contrast, the predictions seem to underestimate the d_{EM} in the middle section, especially for the Slim Straight array. However, differences between measured and predicted d_{EM} were significant only in the apical section of the array (1.04 ± 0.49 mm *vs.* 1.52 ± 0.48, p < 0.001). In the middle (1.41 ± 0.55 mm *vs* 1.27 ± 0.47 mm, p = 0.07) and basal (1.17 ± 0.56 vs. 1.09 ± 0.39 mm, p = 0.29) sections of the array no differences were detected. To summarize, the results indicate that across both electrode types used in the clinical setting, there is a moderate correlation between the measured and predicted d_{EM}s. However, when the values were analyzed separately for each electrode type, the correlations decreased considerably.

Table 1
The fixed-effects parameters, their corresponding estimates, standard errors (SE), t- and p-values separately for scalar area (A_{scala}) and electrode-to-medial wall distance (d_{EM}).

A_{scala}				
Parameter	Estimate	SE	t-value	p-value
Intercept	5.8	0.77	7.44	<0.001
FPI	−0.0043	0.0021	−2.0	0.042
LID	−0.096	0.012	−7.9	<0.001
d_{EM}				
Parameter	Estimate	SE	t-value	p-value
Intercept	2.57	0.40	6.38	<0.001
Amplitude	−0.0003	0.0001	−2.89	<0.001
EF_{slope}	0.0041	0.0017	2.36	0.019
FPI	−0.005	0.0016	−3.3	0.001
LID	0.056	0.010	5.54	<0.001

4. Discussion

This study aimed to evaluate how well our models estimate the intracochlear surroundings and position of a CI electrode array, namely through A_{scala} and d_{EM}, based on electric potential measurements. We also aimed to determine how these models generalize from *ex vivo* to *in vivo* conditions. To this end, the electric potential parameters used in the study were compared between living subjects and HTBs. The parametrization of intracochlear electric potentials was successful, and the error percentages were well within ones reported by Vanpoucke et al. (2004a) and Mohan et al. (2024). Significantly lower electric potential peaks were measured from clinical recordings than from the HTBs, irrespective of the electrode array type. The local potentials measured using Z_{fp} were also lower in intraoperative clinical recordings, but as expected, also when the electrode array was farther away from the modiolus (Tan et al., 2014; Pile et al., 2017; Sijgers et al., 2022; Söderqvist et al., 2023). In contrast, EP_{slope} was only affected by the electrode array type, and it was lower (*i.e.*, more negative, indicating a faster decay of the electric potentials) for perimodiolar than for lateral wall electrode arrays. The placement of the reference electrode affects the transimpedance measurements, and the impedances obtained in the earlier HTB study are comparable to those reported by de Rijk et al. (2020). On the other hand, higher Z_{fp}s in the HTBs also suggest that there may be some loss of soft tissue inside the cochlea, allowing the electrode array to lie closer to the bone, which has a higher electrical resistivity than a healthy scala tympani (Briaire and Frijns, 2000). The inner ear sealing was conducted similarly in both living subjects and HTBs by inserting a muscle plug and fibrin glue onto the round window. Outside the cochlea, current flows to the reference electrode mainly through the cranial cavity or scalp (Tran et al., 2015), which are both missing from HTBs. Instead of these structures, the HTBs were soaked in Ringer's solution mimicking perilymph, serving as the conductive medium to the reference electrode. However, in electric impedance models, the current pathways outside the cochlea are typically modeled by a single bulk resistor (Vanpoucke et al., 2004a), and the cochlear structures are likely the main determinant of intracochlear electric potentials, which are used as inputs in the prediction models of the present study.

In the earlier HTB study, approximately half of the variance in A_{scala} and d_{EM} could be explained by the electric potential measurements and linear insertion depth that could be inspected by the surgeon during the surgery (Söderqvist et al., 2023). In that study, a multiple linear regression model was developed, assuming a fixed relationship between the electric potential measurements and either A_{scala} or d_{EM}. As there are likely individual differences between the HTBs, such as the dimensions of the bones and scalae, further augmented by the possibility of varying degrees of soft tissue loss, mixed-effects models accounting for these factors were applied in this study, as in Sijgers et al. (2022). Following this, 67 % of the variance in A_{scala} could be explained by d_{ins} alone.

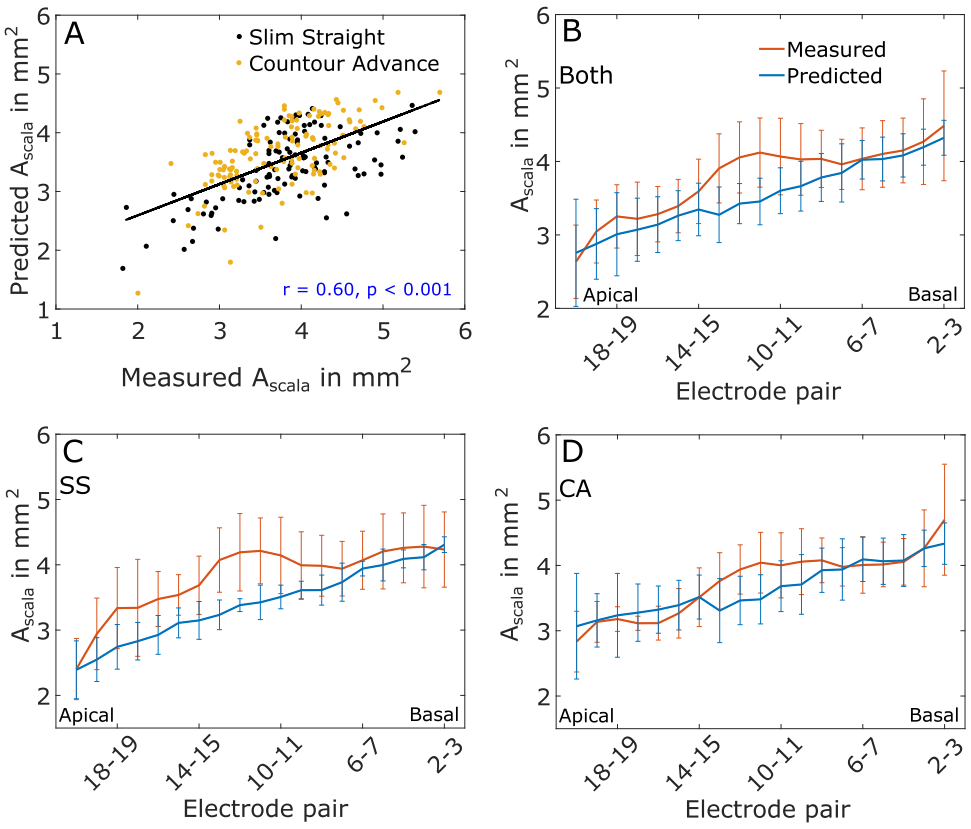

Fig. 1. Comparison of measured and predicted scalar cross-sectional areas (A_{scala}s). A) Comparison of the individual measured and predicted A_{scala}s. Black dots represent Slim Straight (SS) and orange dots Contour Advance). A Pearson's correlation coefficient computed between the variables is shown together with the regression line ($r = 0.60$, $p < 0.001$). B–D) The means and standard deviations (SD) of the measured (orange line) and predicted (blue line) A_{scala}s at the location of each electrode pair arranged from the apical to basal direction for both electrode array types (B) and individually for SS (C) and *CA* (D).

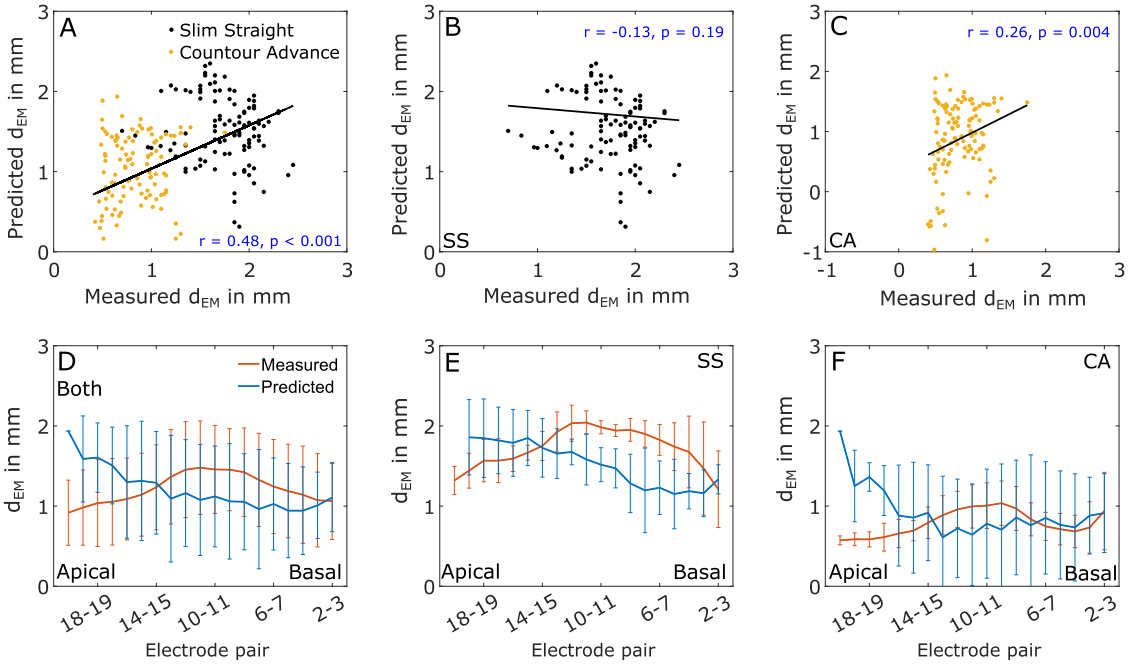

Fig. 2. Comparison of measured and predicted electrode-to-medial wall distances (d_{EM}s). In the upper panel (A–C) are shown the individual measured and predicted d_{EM}s. Black dots represent Slim Straight (SS) and orange dots Contour Advance (*CA*). A) The measured and predicted d_{EM}s for both electrode array types. Pearson's correlation coefficients computed between the variables is shown together with the regression line ($r = 0.50$, $p < 0.001$). B) and C) show individual measured and predicted d_{EM}s for SS and *CA* separately and their respective correlation coefficients are shown ($r = -0.14$, $p = 0.14$ and $r = 0.26$, $p = 0.004$). In the lower panel the means and standard deviations (SD) of the measured (orange line) and predicted (blue line) d_{EM}s at the location of each electrode pair arranged from the apical to basal direction for both electrode array types (D) and individually for SS (E) and *CA* (F).

However, when considering only the fixed effects in the model, the explained variance drastically decreased to 27 %, suggesting that the d_{ins}'s predictive value is heavily influenced by individual differences. Thus, the prediction of A_{scala} depending on d_{ins} alone is not feasible. When Z_{fp} was included in the model, the conditional amount of variance explained by the model increased only slightly to 73 %. However, when considering only the fixed effects, the explained variance improved largely from 27 % to 51 %. For d_{EM}, d_{ins} alone is a poor predictor. Encouragingly, when the electric potential parameters were included in the model, the explained variance increased from 18 % to 65 %, and when considering only the fixed effects, still 50 % of the variance in d_{EM} is explained. These results indicate that including the electric potential measurements in the linear mixed regression models increases explained variance and gives better estimates for A_{scala}s and d_{EM}s.

These developed models, including only the fixed effects, were further used to estimate A_{scala}s and d_{EM}s from clinical electric potential measurements as illustrated in Figs. 1 and 2, respectively. The estimation of A_{scala} was more reliable than for d_{EM} for the clinical data, which is likely due to several reasons. First, the d_{ins} increase and A_{scala} generally decrease monotonously from the basal to apical direction, with the A_{scala} showing a slight decrease between 180° and 360° in the first cochlear turn (Biedron et al., 2010). Since d_{ins} is used as a predictor for both A_{scala} and d_{EM}, this shared monotonic trend results in a more consistent linear relationship between d_{ins} and A_{scala}. In contrast, d_{EM} typically increases from the basal to middle section and then decreases toward the apex (Söderqvist et al., 2023), making the d_{ins}–d_{EM} relationship less linear. Second, A_{scala} is a purely anatomical dimension and independent of electrode type, whereas d_{EM} is strongly influenced by both cochlear anatomy and the type of electrode array used (Ketterer et al., 2018). Also, electrode contacts cause metal artefacts in CBCT images, potentially increasing the apparent electrode diameter by up to 50 % in basal contacts and 70 % in apical contacts (Bevis et al., 2021), which corresponds to an apparent radiological increase of 0.40 and 0.35 mm for the Contour Advance array, respectively. This may lead to overestimation of the d_{EM}, especially in the middle and apical regions for perimodiolar arrays where the true d_{EM} is likely small. Further, the model for d_{EM} depends on successful parametrization of the transimpedances; if this fails, the reliability of the model may be compromised. Finally, in contrast to the HTBs, where the Contour Advance arrays were implanted via the round window approach, these arrays in the living subjects were inserted through a cochleostomy possibly altering the trajectory of the array within the cochlea (Souter et al., 2011). However, the d_{EM} patterns for the Contour Advance appear similar in this study compared to those observed in the HTBs in Söderqvist et al. (2023).

To summarize, the steadily decreasing predicted A_{scala}s from the basal to apical direction may help further confirm the correct insertion and alignment of the electrode array within the intracochlear space alongside visual inspection of TIM heatmaps. Since electric potential measurements are routinely recorded in many clinics and the estimation process can be fully automated, no additional measurements or intraoperative time are needed. The results for predicting d_{EM} based on electric potential measurements are promising but indicate the need for different models for separate electrode array types. Also, the models use electric potential measurements from a single electrode contact to predict the scalar area around it or its distance from the medial wall. Although the parametrized TIM parameters are derived from the measurements from all non-stimulating electrode contacts across the electrode array and Z_{fp} is measured using four adjacent electrodes, future models could benefit from incorporating these variables also from the adjacent contacts to enhance prediction accuracy, since the sequence of electrode contacts is fixed and their locations depend on neighboring electrodes. Successful d_{EM} models could be used to evaluate the optimal electrode array position during the surgery and may help CI programming at the follow-up appointments. Also, as there were significant differences between *vivo* and *ex vivo* electric potential parameters, the accuracy of both models could probably be increased by computing the models using only *in vivo* measurements.

5. Conclusion

An *ex vivo* model may be utilized *in vivo* electric potential measurements to predict cochlear anatomy, despite absolute differences in transimpedances between living subjects and HTBs. Our results suggest that electric potential measurements in combination with d_{ins} can be used to predict A_{scala} with good accuracy, and they may help confirm the correct intracochlear alignment of the electrode array. While the results in d_{EM} prediction are promising, further investigations are required before clinical applications are feasible.

CRediT authorship contribution statement

Samuel Söderqvist: Writing – original draft, Visualization, Validation, Software, Project administration, Methodology, Formal analysis, Data curation, Conceptualization. **Ville Sivonen:** Writing – original draft, Validation, Software, Methodology, Conceptualization. **Alexander Huber:** Supervision, Resources, Project administration, Methodology, Investigation, Conceptualization. **Saku T. Sinkkonen:** Writing – original draft, Validation, Supervision, Methodology, Investigation, Formal analysis, Conceptualization. **Leanne Sijgers:** Writing – original draft, Resources, Project administration, Methodology, Investigation, Formal analysis, Data curation, Conceptualization.

Declarations of interest

None.

Acknowledgements

None

During the preparation of this work the authors used ChatGPT (May 2025 version, OpenAI) in order to edit language and improve clarity of expression. After using this tool, the authors reviewed and edited the content as needed and take full responsibility for the content of the publication.

Data availability

The data that has been used is confidential.

References

Aebischer, P., Meyer, S., Caversaccio, M., Wimmer, W., 2021. Intraoperative impedance-based estimation of Cochlear implant electrode array insertion depth. IEEE Trans. Biomed. Eng. 68, 545–555. https://doi.org/10.1109/TBME.2020.3006934.

Avasarala, V.S., Jinka, S.K., Jeyakumar, A., 2021. Complications of cochleostomy *versus* round window surgical approaches: a systematic review and meta-analysis. Cureus. 14, e25451. https://doi.org/10.7759/cureus.25451.

Bai, S., Encke, J., Obando-Leitón, M., Weiß, R., Schäfer, F., Eberharter, J., Böhnke, F., Hemmert, W., 2019. Electrical stimulation in the Human cochlea: a computational study based on high-resolution micro-CT scans. Front. Neurosci. 13, 1312. https://doi.org/10.3389/fnins.2019.01312.

Berenstein, C.K., Vanpoucke, F.J., Mulder, J.J.S., Mens, L.H.M., 2010. Electrical field imaging as a means to predict the loudness of monopolar and tripolar stimuli in cochlear implant patients. Hear. Res. 270, 28–38. https://doi.org/10.1016/j.heares.2010.10.001.

Biedron, S., Prescher, A., Ilgner, J., Westhofen, M., 2010. The internal dimensions of the cochlear scalae with special reference to Cochlear electrode insertion trauma. Otol. Neurotol. 31, 731–737. https://doi.org/10.1097/MAO.0b013e3181d27b5e.

Bingabr, M., Espinoza-Varas, B., Loizou, P.C., 2008. Simulating the effect of spread of excitation in cochlear implants. Hear. Res. 241, 73–79. https://doi.org/10.1016/j.heares.2008.04.012.

Briaire, J.J., Frijns, J.H.M., 2000. Field patterns in a 3D tapered spiral model of the electrically stimulated cochlea. Hear. Res. 148, 18–30. https://doi.org/10.1016/S0378-5955(00)00104-0.

Cohen, L.T., Richardson, L.M., Saunders, E., Cowan, R.S.C., 2003. Spatial spread of neural excitation in cochlear implant recipients: comparison of improved ECAP method and psychophysical forward masking. Hear. Res. 179, 72–87. https://doi.org/10.1016/S0378-5955(03)00096-0.

Collins, A., Foghsgaard, S., Druce, E., Margani, V., Mejia, O., O'Leary, S., 2024. The effect of electrode position on behavioral and electrophysiologic measurements in perimodiolar cochlear implants. Otol. Neurotol. 45, 238–244. https://doi.org/10.1097/MAO.0000000000004080.

Cottrell, J., Winchester, A., Friedmann, D., Jethanamest, D., Spitzer, E., Svirsky, M., Waltzman, S.B., Shapiro, W.H., McMenomey, S., Roland, J.T., 2024. Characterizing Cochlear implant trans-impedance matrix heatmaps in patients with abnormal anatomy. Otol. Neurotol. 45, e630–e638. https://doi.org/10.1097/MAO.0000000000004304.

de Rijk, S.R., Tam, Y.C., Carlyon, R.P., Bance, M.L., 2020. Detection of extracochlear electrodes in Cochlear implants with electric field imaging/transimpedance measurements: a Human cadaver study. Ear Hear. 2020, 12. https://doi.org/10.1097/AUD.0000000000000837.

Dietz, A., Wennström, M., Lehtimäki, A., Löppönen, H., Valtonen, H., 2016. Electrode migration after cochlear implant surgery: more common than expected? Eur. Arch. Otorhinolaryngol. 273, 1411–1418. https://doi.org/10.1007/s00405-015-3716-4.

Ding, L., Zhang, L., Li, J., Lin, T., 2023. Electrode−modiolus distance affects speech perception for lateral wall electrodes. Otol. Neurotol. 44, e702–e709. https://doi.org/10.1097/MAO.0000000000004019.

Dong, Y., Briaire, J.J., Siebrecht, M., Stronks, H.C., Frijns, J.H.M., 2021. Detection of translocation of cochlear implant electrode arrays by Intracochlear impedance measurements. Ear Hear. 42, 1397–1404. https://doi.org/10.1097/AUD.0000000000001033.

Fitzgerald, M.B., Shapiro, W.H., McDonald, P.D., Neuburger, H.S., Ashburn-Reed, S., Immerman, S., Jethanamest, D., Thomas Roland, J., Svirsky, M.A., 2007. The effect of perimodiolar placement on speech perception and frequency discrimination by cochlear implant users. Acta Otolaryngol. (Stockh.) 127, 378–383. https://doi.org/10.1080/00016480701258671.

Friesen, L.M., Shannon, R.V., Baskent, D., Wang, X., 2001. Speech recognition in noise as a function of the number of spectral channels: comparison of acoustic hearing and cochlear implants. J. Acoust. Soc. Am. 110, 1150–1163. https://doi.org/10.1121/1.1381538.

Giardina, C.K., Krause, E.S., Koka, K., Fitzpatrick, D.C., 2018. Impedance measures during *in vitro* Cochlear implantation predict array positioning. IEEE Trans. Biomed. Eng. 65, 327–335. https://doi.org/10.1109/TBME.2017.2764881.

Helmstaedter, V., Buechner, A., Stolle, S., Goetz, F., Lenarz, T., Durisin, M., 2018. Cochlear implantation in children with meningitis related deafness: the influence of electrode impedance and implant charge on auditory performance – A case control study. Int. J. Pediatr. Otorhinolaryngol. 113, 102–109. https://doi.org/10.1016/j.ijporl.2018.07.034.

Heutink, F., Verbist, B.M., Van Der Woude, W.-J., Meulman, T.J., Briaire, J.J., Frijns, J.H.M., Vart, P., Mylanus, E.A.M., Huinck, W.J., 2021. Factors influencing speech perception in adults with a Cochlear implant. Ear Hear. 42, 949–960. https://doi.org/10.1097/AUD.0000000000000988.

Jiam, N.T., Jiradejvong, P., Pearl, M.S., Limb, C.J., 2016. The effect of round window *vs* cochleostomy surgical approaches on cochlear implant electrode position: a flat-panel computed tomography study. JAMA Otolaryngol. Neck Surg. 142, 873–880. https://doi.org/10.1001/jamaoto.2016.1512.

Joly, C.-A., Reynard, P., Hermann, R., Seldran, F., Gallego, S., Idriss, S., Thai-Van, H., 2021. Intra-cochlear current spread correlates with speech perception in experienced adult Cochlear implant users. J. Clin. Med. 10, 5819. https://doi.org/10.3390/jcm10245819.

Kopsch, A.C., Wagner, L., Plontke, S.K., Kösling, S., 2024. A case series suggests peaking transimpedance as a possible marker for scalar dislocations in cochlear implantation. Audiol. Neurotol. 1–10. https://doi.org/10.1159/000541954.

Labadie, R.F., Noble, J.H., Hedley-Williams, A.J., Sunderhaus, L.W., Dawant, B.M., Gifford, R.H., 2016. Results of postoperative, CT-based, electrode deactivation on hearing in prelingually deafened adult cochlear implant recipients. Otol. Neurotol. 37, 137. https://doi.org/10.1097/MAO.0000000000000926.

Landsberger, D.M., Padilla, M., Srinivasan, A.G., 2012. Reducing current spread using current focusing in cochlear implant users. Hear. Res. 284, 16–24. https://doi.org/10.1016/j.heares.2011.12.009.

Leblans, M., Sismono, F., Vanpoucke, F., Van Dinther, J., Lerut, B., Kuhweide, R., Offeciers, E., Zarowski, A., 2022. Novel impedance measures as biomarker for intracochlear fibrosis. Hear. Res. 426, 108563. https://doi.org/10.1016/j.heares.2022.108563.

Lei, I.M., Jiang, C., Lei, C.L., de Rijk, S.R., Tam, Y.C., Swords, C., Sutcliffe, M.P.F., Malliaras, G.G., Bance, M., Huang, Y.Y.S., 2021a. 3D printed biomimetic cochleae and machine learning co-modelling provides clinical informatics for cochlear implant patients. Nat. Commun. 12, 6260. https://doi.org/10.1038/s41467-021-26491-6.

Lei, I.M., Jiang, C., Lei, C.L., De Rijk, S.R., Tam, Y.C., Swords, C., Sutcliffe, M.P.F., Malliaras, G.G., Bance, M., Huang, Y.Y.S., 2021b. 3D printed biomimetic cochleae and machine learning co-modelling provides clinical informatics for cochlear implant patients. Nat. Commun. 12, 6260. https://doi.org/10.1038/s41467-021-26491-6.

Malherbe, T.K., Hanekom, T., Hanekom, J.J., 2016. Constructing a three-dimensional electrical model of a living cochlear implant user's cochlea. Int. J. Numer. Methods Biomed. Eng. 32, e02751. https://doi.org/10.1002/cnm.2751.

Malherbe, T.K., Hanekom, T., Hanekom, J.J., 2015. The effect of the resistive properties of bone on neural excitation and electric fields in cochlear implant models. Hear. Res. 327, 126–135. https://doi.org/10.1016/j.heares.2015.06.003.

Mohan, P., Sinkkonen, S.T., Sivonen, V., 2024. The association of intraoperative electric field and neural excitation patterns of the cochlear implant with patient-related factors of age, gender, cochlear diameter, and postoperative speech measures. Hear. Res. 453, 109131. https://doi.org/10.1016/j.heares.2024.109131.

Peters, J.P.M., Bennink, E., van Zanten, G.A., 2019. Comparison of place-versus-pitch mismatch between a perimodiolar and lateral wall cochlear implant electrode array in patients with single-sided deafness and a Cochlear implant. Audiol. Neurotol. 24, 38–48. https://doi.org/10.1159/000499154.

Pile, J., Sweeney, A.D., Kumar, S., Simaan, N., Wanna, G.B., 2017. Detection of modiolar proximity through bipolar impedance measurements 7.

Ramos de Miguel, Á., Argudo, A.A., Borkoski Barreiro, S.A., Falcón González, J.C., Ramos Macías, A., 2018. Imaging evaluation of electrode placement and effect on electrode discrimination on different cochlear implant electrode arrays. Eur. Arch. Otorhinolaryngol. 275, 1385–1394. https://doi.org/10.1007/s00405-018-4943-2.

Razmovski, T., Bester, C., Collins, A., O'Leary, S.J., 2022. Four-point impedance changes in the early post-operative period after Cochlear implantation. Otol. Neurotol. 43, e730–e737. https://doi.org/10.1097/MAO.0000000000003592.

Saoji, A.A., DeJong, M.D., Bertsch, N.J., Graham, M.K., Goulson, K.R., Wernsman Pease, M.L., Gruenwald, J.M., Bross, A.E., Dornhoffer, J.R., Neff, B.A., Driscoll, C.L.W., Carlson, M.L., Lane, J.I., Pesch, J., Vanpoucke, F.J., 2024. Pathophysiology of facial nerve stimulation and its implications for electrical stimulation in cochlear implants. Otol. Neurotol. 45, e84–e90. https://doi.org/10.1097/MAO.0000000000004082.

Schraivogel, S., Aebischer, P., Wagner, F., Weder, S., Mantokoudis, G., Caversaccio, M., Wimmer, W., 2023. Postoperative impedance-based estimation of Cochlear implant electrode insertion depth. Ear Hear. 44, 1379–1388. https://doi.org/10.1097/AUD.0000000000001379.

Sijgers, L., Geys, M., Geissler, G., Boyle, P., Huber, A., Pfiffner, F., 2024. Electrical bioimpedance-based monitoring of intracochlear tissue changes after cochlear implantation. Sensors 24, 7570. https://doi.org/10.3390/s24237570.

Sijgers, L., Huber, A., Tabibi, S., Grosse, J., Roosli, C., Boyle, P., Koka, K., Dillier, N., Pfiffner, F., Dalbert, A., 2022. Predicting Cochlear implant electrode placement using monopolar, three-point and four-point impedance measurements. IEEE Trans. Biomed. Eng. 69, 2533–2544. https://doi.org/10.1109/TBME.2022.3150239.

Söderqvist, S., Sinkkonen, S.T., Sivonen, V., 2022. The intraoperative relationship between intracochlear electrical field and excitability of the auditory nerve. Heliyon. 8, e11970. https://doi.org/10.1016/j.heliyon.2022.e11970.

Söderqvist, S., Sivonen, V., Koivisto, J., Aarnisalo, A., Sinkkonen, S.T., 2023. Spread of the intracochlear electrical field: implications for assessing electrode array location in cochlear implantation. Hear. Res. 434, 108790. https://doi.org/10.1016/j.heares.2023.108790.

Souter, M.A., Briggs, R.J., Wright, C.G., Roland, P.S., 2011. Round window insertion of precurved perimodiolar electrode arrays: how successful is it? Otol. Neurotol. 32 (1), 58–63. https://doi.org/10.1097/MAO.0b013e3182009f52.

Tan, C.-T., Svirsky, M., Anwar, A., Kumar, S., Caessens, B., Carter, P., Treaba, C., Thomas, J., Jr, R., 2014. Real-time measurement of electrode impedance during intracochlear electrode insertion 17. https://doi.org/10.1002/lary.23714.

Tran, P., Sue, A., Wong, P., Li, Q., Carter, P., 2015. Development of HEATHER for Cochlear implant stimulation using a new modeling workflow. IEEE Trans. Biomed. Eng. 62, 728–735. https://doi.org/10.1109/TBME.2014.2364297.

Van Weert, S., Stokroos, R.J., Rikers, M.M.J.G., Van Dijk, P., 2005. Effect of perimodiolar cochlear implant positioning on auditory nerve responses: a neural response telemetry study. Acta Otolaryngol. (Stockh.) 125, 725–731. https://doi.org/10.1080/00016480510028492.

Vanpoucke, F., Zarowski, A., Casselman, J., Frijns, J., Peeters, S., 2004a. The facial nerve canal: an important cochlear conduction path revealed by clarion electrical field imaging. Otol. Neurotol. 25, 282–289. https://doi.org/10.1097/00129492-200405000-00014.

Vanpoucke, F.J., Boermans, P.B., Frijns, J.H., 2012. Assessing the placement of a Cochlear electrode array by multidimensional scaling. IEEE Trans. Biomed. Eng. 59, 307–310. https://doi.org/10.1109/TBME.2011.2173198.

Vanpoucke, F.J., Zarowski, A.J., Peeters, S.A., 2004b. Identification of the impedance model of an implanted cochlear prosthesis from intracochlear potential measurements. IEEE Trans. Biomed. Eng. 51, 2174–2183. https://doi.org/10.1109/TBME.2004.836518.

Wanna, G.B., Noble, J.H., Carlson, M.L., Gifford, R.H., Dietrich, M.S., Haynes, D.S., Dawant, B.M., Labadie, R.F., 2014. Impact of electrode design and surgical approach on scalar location and cochlear implant outcomes. Laryngoscope 124, S1–S7. https://doi.org/10.1002/lary.24728.

Wilk, M., Hessler, R., Mugridge, K., Jolly, C., Fehr, M., Lenarz, T., Scheper, V., 2016. Impedance changes and fibrous tissue growth after cochlear implantation are correlated and can Be reduced using a dexamethasone eluting electrode. PLoS. One 11, e0147552. https://doi.org/10.1371/journal.pone.0147552.

Zhang, L., Schmidt, F.H., Oberhoffner, T., Ehrt, K., Cantré, D., Großmann, W., Schraven, S.P., Mlynski, R., 2024. Transimpedance matrix can Be used to estimate electrode positions intraoperatively and to monitor their positional changes postoperatively in Cochlear implant patients. Otol. Neurotol. 45, e289–e296. https://doi.org/10.1097/MAO.0000000000004145.

Zuniga, M.G., Rivas, A., Hedley-Williams, A., Gifford, R.H., Dwyer, R., Dawant, B.M., Sunderhaus, L.W., Hovis, K.L., Wanna, G.B., Noble, J.H., Labadie, R.F., 2017. Tip fold-over in Cochlear implantation: case series. Otol. Neurotol. 38, 199–206. https://doi.org/10.1097/MAO.0000000000001283.